Article

Neuron

Collateral Pathways from the Ventromedial Hypothalamus Mediate Defensive Behaviors

Highlights

- Activating VMHdm/c SF1 cells induces defensive-like motor and autonomic responses
- The VMH→PAG and VMH→AHN pathways mediate immobility and avoidance, respectively
- VMHdm/c neurons send collateral projections to the AHN and dlPAG
- AHN activation elicits escape jumping and avoidance, but not immobility

Authors

Li Wang, Irene Z. Chen, Dayu Lin

Correspondence

dayu.lin@nyumc.org

In Brief

Wang et al. show that SF1-expressing cells in the ventromedial hypothalamus (VMH) mediate complex defense-like somatomotor and autonomic responses. Collateral projections from the VMH to different downstream regions mediate distinct aspects of defense, suggesting a one-to-many and nonredundant circuit configuration.

Wang et al., 2015, Neuron *85*, 1344–1358
March 18, 2015
http://dx.doi.org/10.1016/j.neuron.2014.12.025

CellPress

CellPress

Neuron
Article

Collateral Pathways from the Ventromedial Hypothalamus Mediate Defensive Behaviors

Li Wang,[1] Irene Z. Chen,[1] and Dayu Lin[1,2,3,4,*]
[1]Institute of Neuroscience, New York University School of Medicine, 522 First Avenue, New York, NY 10016, USA
[2]Department of Psychiatry, New York University School of Medicine, 1 Park Avenue, New York, NY 10016, USA
[3]Center for Neural Science, New York University, 4 Washington Place, New York, NY 10003, USA
[4]The Nathan Kline Institute for Psychiatric Research, 140 Old Orangeburg Road, Orangeburg, NY 10962, USA
*Correspondence: dayu.lin@nyumc.org
http://dx.doi.org/10.1016/j.neuron.2014.12.025

SUMMARY

The ventromedial hypothalamus (VMH) was thought to be essential for coping with threat, although its circuit mechanism remains unclear. To investigate this, we optogenetically activated steroidogenic factor 1 (SF1)-expressing neurons in the dorsomedial and central parts of the VMH (VMHdm/c), and observed a range of context-dependent somatomotor and autonomic responses resembling animals' natural defensive behaviors. By activating independent pathways emanating from the VMHdm/c, we demonstrated that VMHdm/c projection to the dorsolateral periaqueductal gray (dlPAG) induces inflexible immobility, while the VMHdm/c to anterior hypothalamic nucleus (AHN) pathway promotes avoidance. Consistent with the behavior changes induced by VMH to AHN pathway activation, direct activation of the AHN elicited avoidance and escape jumping, but not immobility. Retrograde tracing studies revealed that nearly 50% of PAG-projecting VMHdm/c neurons send collateral projection to the AHN and vice versa. Thus, VMHdm/c neurons employ a one-to-many wiring configuration to orchestrate multiple aspects of defensive behaviors.

INTRODUCTION

Many species develop coping strategies to avoid danger and to survive. Given that these defensive reactions are innate, the neural mechanism underlying these behaviors is likely hardwired. The hypothalamus plays a critical role in the expression of defense behavior (Bard, 1928). Decorticated cats display a mixed pattern of rage and defense responses, such as hissing and paw striking, only if the caudal hypothalamus is left intact. Conversely, classic electric and chemical stimulation experiments demonstrated that a pattern of somatomotor and autonomic responses that resemble the behavior of animals facing natural threats can be elicited from the medial hypothalamus in many species, including human (Fernandez De Molina and Hunsperger, 1962; Lammers et al., 1988; Lipp and Hunsperger, 1978; Schmitt et al., 1985; Silveira and Graeff, 1988; Wilent et al., 2010). In fact, there appears to be an interconnected hypothalamic defense circuitry, which comprises the anterior hypothalamic nucleus (AHN), the dorsomedial part of the ventromedial hypothalamus (VMHdm), and the dorsal part of the premammillary nucleus (PMd), that shows strong immediate-early gene responses in rats and mice exposed to live predators (Canteras et al., 1994; Canteras and Swanson, 1992; Dielenberg et al., 2001; Martinez et al., 2008; Risold et al., 1994). Recently, manipulations focusing on the dorsomedial and central parts of the VMH (VMHdm/c) showed that pharmacogenetic inactivation of the area reduces freezing and head-out responses to a natural predator (Silva et al., 2013), while optogenetic activation of VMH cells could elicit immobility, especially when the manipulated area involves the VMHdm/c (Lin et al., 2011). This suggests that the VMHdm/c acts as an essential relay in innate defense.

The exact role of the VMHdm/c in defense and its underlying circuit remains unknown. In this study, we found that optogenetic activation of VMHdm/c promotes a variety of context-dependent defense-like somatomotor and autonomic responses. Furthermore, we examined the role of two pathways from the VMHdm/c in mediating these behaviors: the main ascending projection to the AHN (a key component of the hypothalamic defense circuitry) and the main descending projection to the dorsolateral periaqueductal gray (dlPAG, a midbrain structure known for its involvement in defensive responses) (Brandão et al., 2008; Canteras et al., 1994; Martinez et al., 2008). We found that, although a substantial portion of VMHdm/c neurons send collateral projections to the AHN and the dlPAG, these two pathways mediate distinct aspects of defensive responses. Whereas activation of the VMH→AHN pathway elicits avoidance, activation of the VMH→PAG pathway elicits immobility, but not avoidance. Consistent with the pathway activation result, direct activation of AHN cells elicits avoidance, but no immobility. Thus, we conclude that VMHdm/c neurons orchestrate instantaneous stereotyped immobility and flexible escaping, at least in part, through their collateral descending projection to the PAG and ascending projection to the AHN.

RESULTS

VMHdm/c Stimulation Induces Activity and Context-Dependent Defensive Behavior

To manipulate VMHdm/c cells, we used a well-characterized transgenic line that expresses CRE recombinase under the

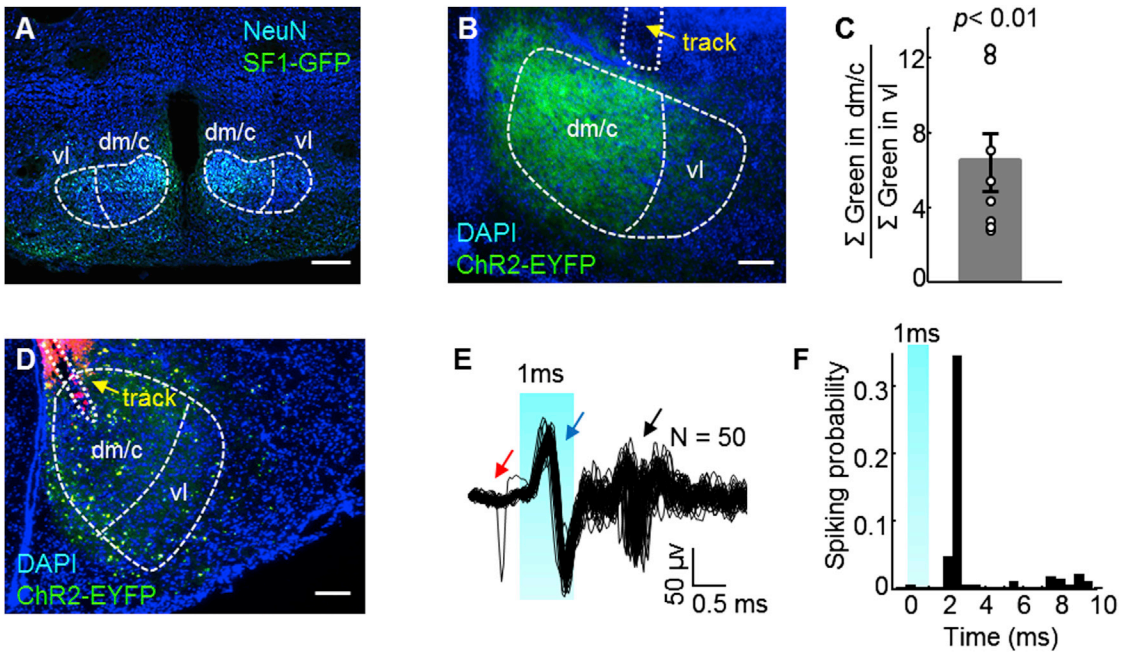

Figure 1. Optogenetic Stimulation of SF1 Neurons in the VMHdm/c Induced Spiking Activity

(A) GFP (green) staining reveals SF1-positive cells in the VMH of an SF1:CRE × RCE:loxP mouse. Blue, NeuN. Scale bar, 500 μm.

(B) Virally expressed ChR2-EYFP (green) is concentrated in the VMHdm/c. Blue, DAPI. Scale bar, 200 μm.

(C) The ratio of accumulated pixel values of EYFP expression (green channel) in the VMHdm/c relative to in the VMHvl (n = 8) is significantly more than one (Student's t test). Error bar, SE. Each dot represents data from one animal.

(D) Optrode (yellow arrow) track in the VMHdm/c. Green, ChR2-EYFP; blue, DAPI; red, DiI painted on the optrode. Scale bar, 200 μm.

(E) The 50 overlaid electrophysiological traces aligned to the 1 ms light onset. Red arrow, spontaneous spike; black arrow, evoked spikes; blue arrow, stimulation artifacts.

(F) Spiking probability (number of spikes/number of trials) aligned to the light onset. Bin size, 0.5 ms; blue shading, light on.

regulation of the SF1 promoter (Dhillon et al., 2006). In the CNS, SF1 expression is largely limited in the VMH (McClellan et al., 2006). By crossing the SF1:CRE line with a GFP reporter line, we observed that 58.5% of VMHdm/c cells and 47.2% of VMHvl cells are GFP-positive (Figure 1A, n = 3). In combination with precise stereotactic injection of CRE-dependent virus, we limited our exogenous protein expression primarily to the VMHdm/c (Figures 1B and 1C). We tested whether spiking activity could be induced by light activation of SF1 neurons that express channelrhodopsin (ChR2) (Boyden et al., 2005). Two weeks after injecting adeno-associated virus (AAV)-expressing CRE-dependent ChR2-EYFP into the VMHdm/c of SF1:CRE mouse, we delivered pulsed blue light (473 nm, 5 Hz, 1 ms) through an implanted optrode, and observed reliable light-evoked spikes in the VMHdm/c (Figures 1D–1F).

We next tested the behavioral changes induced by light activation of VMHdm/c SF1 neurons. In the animals' home cage, blue light delivery (1 mW, 20 Hz, 20 ms) immediately reduced or completely suppressed the animals' movement. As the light intensity increased (up to 6 mW), we noticed that some animals started to run along the perimeter of the cage after initial immobility, and sometimes showed repeated wall rearing and escape jumping (12/31). Figures 2A and 2B show all 31 animals' behavior induced by high-intensity light. Figure 2C shows eight animals that exhibited jumping under high-intensity light and were systematically tested with low-intensity light (Movie S1). At the offset of the 60 s stimulation, the animal often appeared agitated for 10–60 s, as indicated by its significantly increased movement velocity (Figure S1A). To quantify these behavioral changes, we tracked animal's body center location (Burgos-Artizzu et al., 2012; Dollar et al., 2010). Then, we calculated the movement velocity at the xy plane with top-view tracking and the vertical movement velocity and elevation with side-view tracking (Figures S2A and S2B). For a given frame, immobility, running, and jumping episodes were then detected based on the combined measures of instantaneous velocity and location of the animal. The performance of our automated behavioral detection program was validated by comparison with human annotation (Figures S2C–S2F).

The running and jumping responses increased with stimulation intensity (Figure 2C) and frequency (Figure 2G). In the 12 animals that we observed light-induced jumping in at least one trial, low-frequency stimulation (5–10 Hz) primarily induced immobility (on average, 67.2% of total stimulation time), some running (33.1% of all trials), and rarely jumping (4.2% of all trials). Increasing the stimulation frequency to high (15–20 Hz) significantly reduced the immobility time (on average, 40.4% of total stimulation time), while it increased both running (94.2% of all trials) and jumping events (73.6% of all trials) (Figures 2D–2G). Increased stimulation frequency also decreased the latency to running

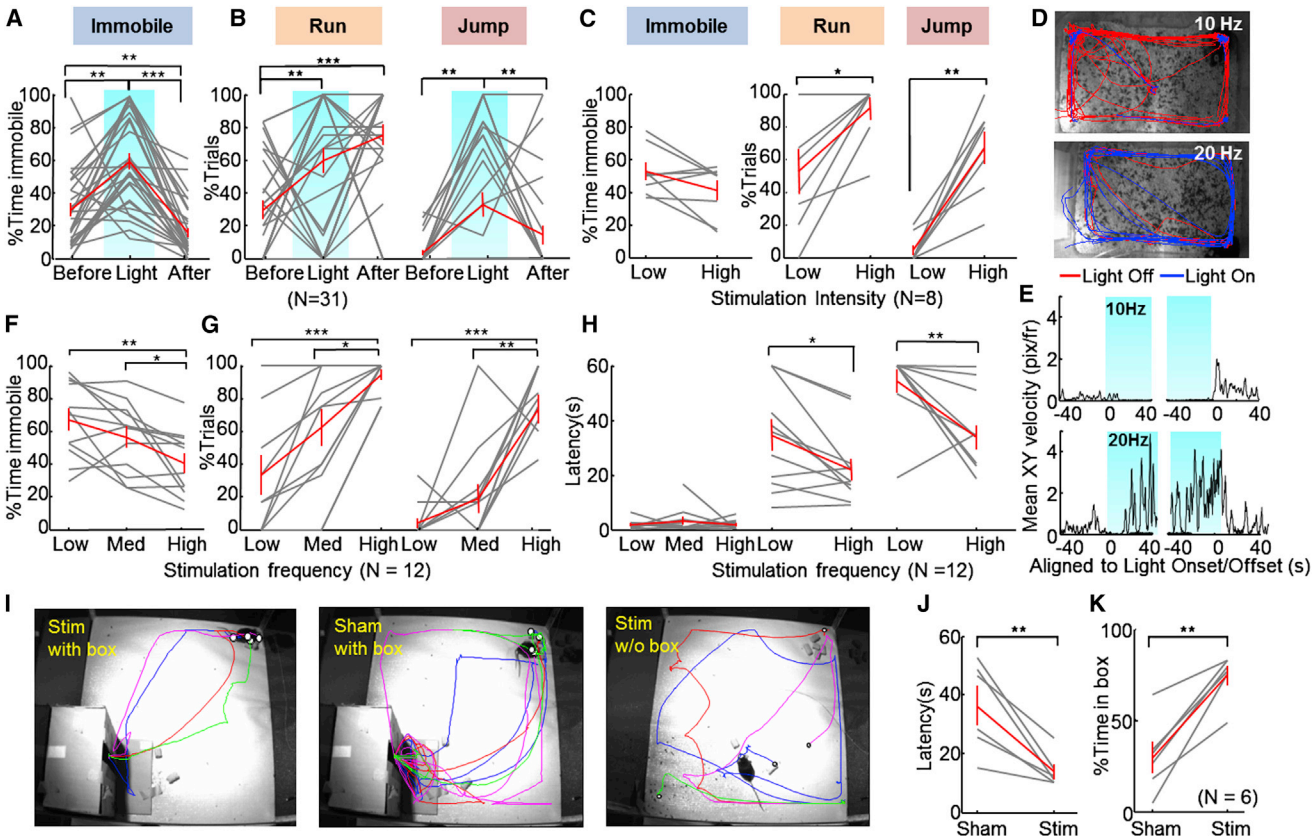

Figure 2. Optogenetic Stimulation of SF1 Neurons in VMHdm/c Induced Defensive Behaviors

(A and B) The average percentage of time that the animal spent immobile (A) and the average percentage of trials with running and jumping events (B) were significantly higher during light delivery (n = 31).

(C) Increased light intensity increased the percentage of trials with running and jumping events, but did not significantly change the time of immobility (n = 8).

(D) Examples of tracking traces with 10 Hz (five trials) and 20 Hz (six trials) light pulses. Blue and red traces are the light on and off periods, respectively.

(E) Peristimulus time histograms (PSTHs) of locomotion velocity aligned to the 10 Hz (top) and 20 Hz (bottom) stimulation onset (left, blue shading) and offset (right, blue shading).

(F–H) Increases in light-pulse frequency decreased the time spent immobile (F); increased the percentage of trials with running and jumping events (G); and shortened latency to running and jumping, but did not change latency to immobility (H) (n = 12).

(I) Representative tracking traces during the hiding box test. Different colors represent different stimulation trials. The white dot indicates the animal's position at light onset.

(J–K) Light stimulation shortened latency to return to the box (J) and increased total percentage of time in the box (K) (n = 6). Gray and red lines indicate data of individuals and population average, respectively. Error bars, SE. Paired t test: *p < 0.05, **p < 0.01, ***p < 0.001. See also Figures S1 and S2 and Movies S1 and S2.

and jumping significantly, but the latency to immobility remained similar and much shorter (Figure 2H). Thus, VMHdm/c SF1 cell optogenetic activation induced a range of behavioral responses that resemble the animals' reaction to an approaching predator (Blanchard et al., 1998). The exact form of response depends on both the frequency and intensity of the light, which presumably affect the spiking rate and the number of activated cells, respectively.

When a prey animal encounters a predator, its defensive reaction depends on the distance from the predator as well as the availability of a shelter. If a shelter is nearby, the most likely adopted defensive strategy is hiding (Blanchard et al., 1995; Eilam, 2005). To test whether activation of SF1 neurons can induce hiding, we examined the behavior response of the animal when the light was delivered in a large arena containing a hiding box (Figure 2I). During the test, animals first freely explored the arena for 10 min. Thereafter, interleaved sham and real stimulations were initiated when the animal reached a designated corner far from the hiding box (Figure 2I). We found that, although light stimulation sometimes induced immobility briefly, all animals quickly took a direct route back to the hiding box (Figure 2I; Movie S2). Across animals, the latency to the hiding box during real stimulation was significantly shorter than that during sham stimulation (Figure 2J). Once reaching the hiding box, the animal stayed inside of the box despite continued light stimulation. As a result, the animal spent approximately 75% of time in the hiding box during real stimulation but less than 30% during sham stimulation (Figure 2K). If the stimulation started when the animal was

already in the box, the animal remained in the box for the entire stimulation period (eight trials from three animals). In contrast, in the absence of a hiding box, the stimulation induced immobility and sometimes running from corner to corner (Figure 2I), both of which are behaviors similar to those observed in the home cage (Figure 2A). Taken together, VMHdm/c SF1 cell activation did not elicit a set of stereotyped motor actions, but instead induced defensive behaviors suitable for the environment.

VMHdm/c SF1 Cell Stimulation Induced Autonomic Responses

The defensive reaction in the face of danger is not only reflected in the motor response but also involves concomitant neuroautonomic adjustment. Thus, we next measured changes in heart rate (HR), breathing rhythm, and pupillary size during VMHdm/c SF1 cell stimulation. In a head-fixed preparation, we recorded the pupil response in awake animal and found that pupil diameter increased by approximately one-third during light activation and gradually returned to the baseline over 10–20 s after light offset (Figure 3A; Movie S3). The slow recovery of pupil size after light stimulation might result partly from an increase in postlight locomotion, given that we noticed pupil dilation during spontaneous movement in the absence of stimulation (Figure 3B). However, the sharp increase in pupil size during light exposure is not movement-related, as locomotion is largely suppressed during light. In addition, the breathing rate also increased by approximately one-third during stimulation (Figure 3D). Increasing light intensity sometimes increased the response magnitude, but never changed the response direction (Figures 3A, 3C, and 3D). These light-evoked pupillary and respiratory responses are consistent with those observed during natural danger exposure, indicating the activation of a sympathetic nervous system (Hofer, 1970; Höfle et al., 2013).

We also measured the light-induced cardiovascular response in freely moving animals using chronically implanted electrodes (Figure 3E). At low light intensity (0.8–1.7 mW), stimulation induced a significant increase in HR and decreased heart rate variability (HRV) in all but one animal (5/6) (Figures 3F–3J). However, when the light intensity increased (2.5–5 mW), the light-induced HR response changed. For those five animals that showed a tachycardia response under low light, the HR remained increased under high-intensity light for one animal, decreased in two animals, and changed variably in the remaining two animals (decreased for some but not all trials) (Figures 3F–3J). One animal (1/6) showed a bradycardia response under both low- and high-intensity light (Figures 3I and 3J). The light-induced tachycardia and bradycardia responses have different kinetics. For the former, the HR increases gradually after light onset, reaching a plateau in approximately 10 s; at light offset, the HR decreases gradually and returns to the prestimulation level in 15–20 s. In contrast, the light-induced bradycardia response can take 30–40 s to reach a stable level, sometimes as low as half of the baseline rate, and, at light offset, the HR returns to the baseline level nearly instantaneously (Figure 3F). This qualitatively different cardiovascular response under low- and high-intensity light cannot be explained by behavioral difference, as animals showed immobility for at least the first 10–30 s during both light conditions. On the other hand, HR always increases to a high level (~750 bpm) as the animal prepares to run regardless of the stimulation condition (Figure 3K). Thus, SF1 cell activation can induce complex cardiovascular responses depending on the intensity of light stimulation and ongoing behaviors. In general, low-level activation of VMHdm/c SF1 cells induces a tachycardia response, whereas high-level activation induces a bradycardia response.

VMHdm/c Activation Promotes Behavioral Avoidance

The ultimate goal of activating the defense circuit is to survive, and avoidance is a critical strategy. Thus, we next tested whether increased VMHdm/c activity promotes avoidance using a real-time place preference (RTPP) test. During the test, the animal first freely explored an arena with two distinct compartments for 5–10 min prior to any light stimulation. Then, the compartment in which the animal spends more time was assigned as the stimulation chamber. During the 30 min stimulation period, the animal received blue light pulses (3 s on and 2 s off, 20 Hz and 20 ms) whenever it entered the stimulation chamber; the stimulation was turned off when the animal entered the safe chamber and when the 3 s light-on period ran out (Figures 4A and 4B). If the animal failed to exit the stimulation chamber within 3 min, the light was turned off for 15 s before resuming the stimulation protocol.

The stimulation intensity used in the test was relatively low, eliciting only immobility in the home cage. Consistent with the light-induced behavioral changes in the home cage, during initial rounds of entries into the stimulation chamber, test animals increased immobility during light stimulation, and, as a result, might spend hundreds of seconds in the stimulation chamber before exiting (Figure 4C, red arrow; Movie S4). However, after one to three entries, all animals learned that stimulation could be avoided by entering the safe chamber. They significantly decreased the latency to exit the stimulation chamber and increased their time in the safe chamber (Figures 4C–4E). Furthermore, while light stimulation increased immobility initially, 13/18 animals showed no immobility under light delivery during later entries; instead they quickly turned around and exited the stimulation chamber (Figure 4H; Movie S4). Consequently, when stimulation periods are considered altogether, most animals spent less time immobile during stimulation compared with the pretest (Figure 4G). This decreased immobility is opposite to the increased immobility observed in the home cage (Figure 2A), supporting that the VMHdm/c-induced defensive responses are flexible, depending on whether an escape option is available or not. Finally, despite the initial immobility induced by VMHdm/c stimulation that increased the time spent in the stimulation chamber, the total percentage of time in the stimulation chamber over the 30 min testing was significantly reduced across all the animals (n = 18), suggesting that VMHdm/c stimulation promotes avoidance (Figure 4F).

Given that prolonged VMHdm/c stimulation could increase locomotion, we tried to decouple the avoidance behavior from changes in movement using a 2 s low-intensity stimulation protocol in a punishment operant conditioning task (Figures 4I and 4J). When tested in the home cage, the 2 s stimulation slightly reduced animals' movement, but caused no significant change in locomotion after stimulation ($p = 0.135$, paired t test for mean velocity during 10 s before and 10 s after stimulation, a

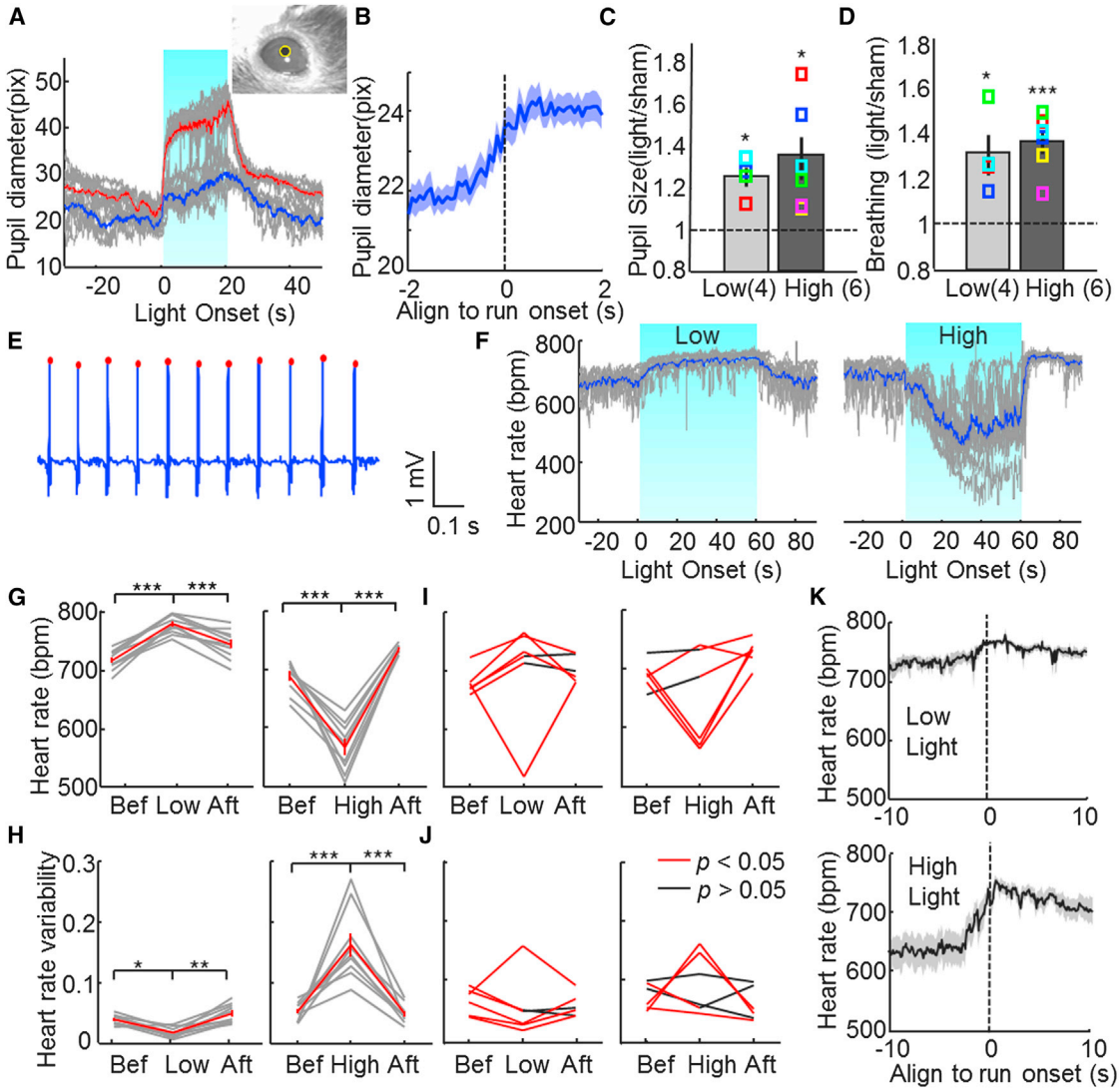

Figure 3. VMH SF1 Neuron Stimulation Induced Autonomic Responses

(A) PSTHs of the pupil diameter aligned to light onset. Gray lines indicate individual trials. Blue and red lines indicate the average response curve under low- (blue) and high- (red) intensity light. Upper right corner shows a representative image with computer-detected pupil (yellow circle).

(B) Pupil diameter aligned to spontaneous running (n = 102 trials; 5 animals).

(C and D) Significantly increased pupil diameter (C) and breathing rate (D) during low- (n = 4) or high- (n = 6) intensity light stimulation. Colored squares show individual animals.

(E) Raw ECG trace with computer-detected heartbeats (red dots).

(F) PSTHs of heart rate aligned to light onset. Note opposite HR response during low- (left) and high- (right) intensity light.

(G and H) HR (top) and HRV (bottom) changes during low- and high-intensity light stimulation of an example animal. Gray, individual trials; red, average.

(I and J) HR (top) and HRV (bottom) changes of all six animals during low- (left) and high- (right) intensity light stimulation. Red line indicates response during light is significantly different from before or after period (FDR adjusted $p < 0.05$, paired t test across trials for each animal).

(K) PSTHs of HR aligned to the onset of running events during either low- (top, n = 11) or high- (bottom, n = 22) intensity light stimulation. See also Movie S3.

total of 189 trials from three animals; Figure 4K). During the punishment operant conditioning task, water-deprived animals first learned to associate nose poking with water reward. Once stable poking performance was achieved (poke number ± 10% for 2 consecutive days), each poke was then followed by a brief light pulse (2 s, 20 Hz, and 20 ms) triggered 0.8 s after poking (Figure 4I). If the stimulation was considered negative, this punishment was expected to reduce the number of pokes. Consistent with the results of RTPP test, pairing the poking with VMHdm/c activation significantly decreased the number of pokes during the 30 min testing session, although the decrease was not maintained when the animals were tested the next day with no light pairing (Figure 4M). The decreased poking could not be accounted for by immobility caused by stimulation, given that most animals continued licking the water spout during stimulation, and on average spent only 20% of the time immobile

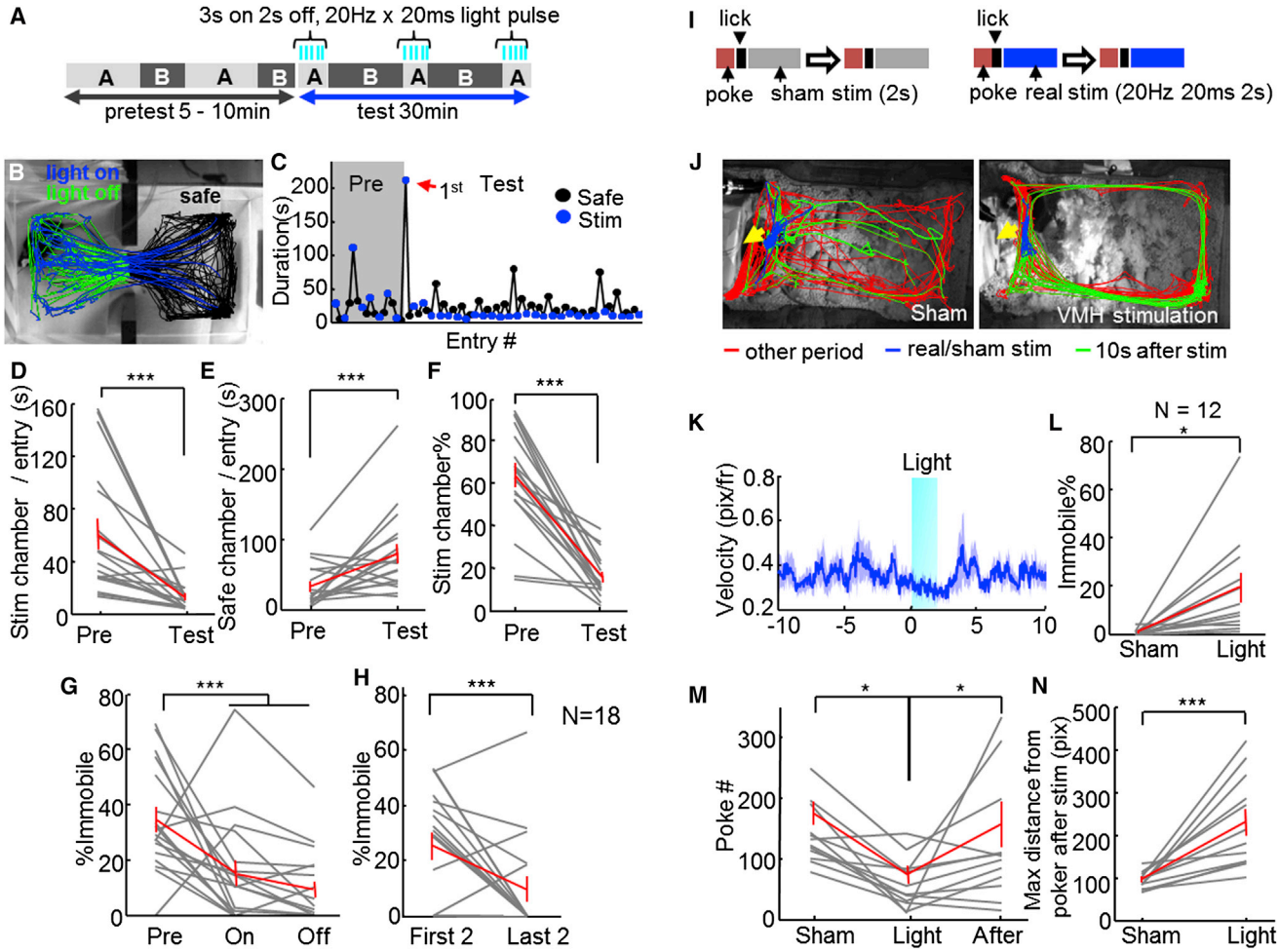

Figure 4. VMH SF1 Neuron Activation Promoted Avoidance

(A) Experimental schematic of RTPP test.

(B) Tracking traces from one test session.

(C) Time spent in safe and stimulation chambers during each entry of the session shown in (B). Red arrow indicates the first entry into the stimulation chamber during test.

(D–F) Stimulation of the VMHdm/c decreased the duration in the stimulation chamber per entry (D), increased the duration in the safe chamber per entry (E), and decreased the percentage of time in the stimulation chamber (F).

(G) The animal spent a smaller percentage of time immobile during and between stimulation compared with the pretest.

(H) Percentage of time immobile during the last two entries to the stimulation chamber was much less than that during the first two entries (D–H) (n = 18).

(I) Schematics of punishment operant conditioning.

(J) Tracking traces during sham (left) and VMH (right) stimulation. Yellow arrows indicate nose ports. Note the limited movement during light stimulation (blue) and increased movement along the perimeter of the cage (green) after stimulation.

(K) Locomotion velocity (mean ± SEM) aligned to the 2 s light stimulation (light blue) onset in the home cage (n = 66 trials from one animal).

(L) Increased immobility during VMH stimulation in comparison to sham stimulation.

(M) The poking number significantly decreased with VMH stimulation but returned to baseline 1 day after stimulation.

(N) Animals moved away from the poker after VMH stimulation (n = 12 for L–N). Gray and red lines indicate results from individual animals and population average, respectively. Error bars, SE. Paired t test: *p < 0.05, ***p < 0.001. See also Movie S4.

(Figure 4L). However, after several paired stimulations, animals moved away from the poker and sometimes stayed in a far corner for hundreds of seconds before poking again (Figure 4N). Taken together, we concluded that VMHdm/c stimulation could induce complex autonomic changes and defense-like motor responses, including immobility, escape jumping, hiding, and avoiding.

Defensive Reactions Induced by Activating the VMH→PAG and VMH→AHN Pathways

To understand the pathways underlying the observed behavioral change, we took advantage of the membrane localization of ChR2-EFYP protein and mapped the terminal fields of the VMHdm/c SF1 neurons. Consistent with previous reports, rostrally, VMHdm/c axons innervate the AHN, periventricular

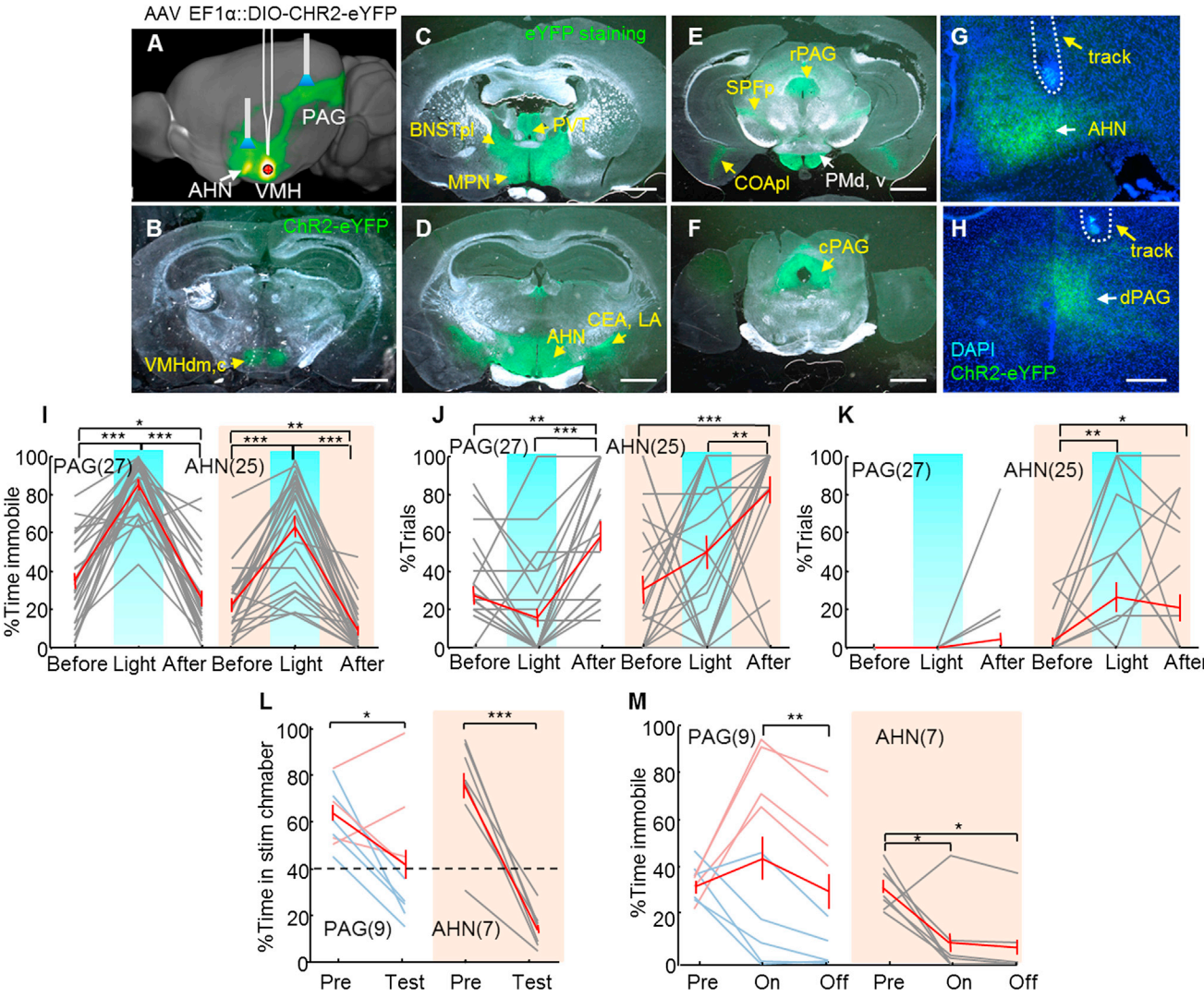

Figure 5. VMH→AHN and VMH→PAG Terminal Stimulation Induced Defense-like Motor Responses and Avoidance

(A) Schematic representation of VMH→AHN and VMH→PAG terminal stimulation. Image adopted from http://connectivity.brain-map.org/, experiment ID: 182337561.

(B) Native expression of EYFP in an SF1:CRE mouse bilaterally injected with AAV2 expressing CRE-dependent ChR2-EFYP.

(C–F) EYFP staining reveals the terminal fields of VMHdm/c SF1 neurons (green). Scale bars in (B–F), 1 mm.

(G and H) An example of fiber terminals (green) and cannula/optic fiber tracks (yellow arrows) in the AHN (G) and the PAG (H). Blue, DAPI. Scale bar, 200 μm.

(I–K) Stimulating the VMH→PAG pathway significantly increased immobility (I, left), but not running (J, left) or jumping (K, left), whereas VMH→AHN axon terminal stimulation increased immobility (I, right), running (J, right), and jumping (K, right).

(L) VMH→AHN terminal stimulation (right) decreased the percentage of time spent in the stimulation chamber in all animals, whereas the VMH→PAG terminal stimulation (left) induced avoidance only in 5/9 animals (light blue lines). Dashed line indicates 40% time in the stimulation chamber.

(M) VMH→AHN stimulation (right) decreased immobility while VMH→PAG stimulation (left) induced heterogeneous changes in immobility. Gray and red lines indicate individual result and population average. (PAG, n = 9; AHN, n = 7). Error bars, SE. Paired t test: *p < 0.05, **p < 0.01, ***p < 0.001. See also Figures S3 and S4 and Movie S5.

nucleus, medial preoptic nucleus (MPN), and posterolateral part of the bed nucleus of stria terminalis (BNSTpl) (Figures 5C and 5D; Canteras et al., 1994; Lindberg et al., 2013). In particular, we noticed that the ventral part of the AHN (sometimes referred to as the lateroanterior hypothalamic nucleus [Franklin and Paxinos, 2008]) contains an especially dense terminal field (Figure 5G). This cluster of axons also can be observed when surveying the online connectivity database (http://connectivity.brain-map.org/, experiment ID: 182337561 using the same SF1:CRE transgenic line; Figure 5A). Dorsally, axons reach the paraventricular thalamic nucleus (Figures 5C and 5D), and, laterally, moderate number of fibers can be observed in the central amygdala, lateral amygdala, medial amygdala (MEA), and posterolateral cortical amygdala (Figures 5D and 5E). Caudally,

the PAG represents the major target of VMHdm/c axons. A large portion of fibers course through the dorsomedial hypothalamus and posterior hypothalamus, and eventually reach the PAG. The remaining axons project ventrally through the PMd and mammillary body, and then take a lateral route through the parvocellular subparafascicular thalamic nucleus to the PAG (Figures 5E and 5F). At the rostral PAG, VMHdm/c axons are concentrated in the dorsal half of the PAG while both the dorsal and ventral caudal PAG are innervated by VMHdm/c fibers (Figures 5E, 5F, and 5H). Taken together, the PAG is the most important target of the VMHdm/c-descending pathway, while the AHN (especially its anterior ventral part) receives dense input from the VMHdm/c-ascending axons and represents the first major target in this direction. Consistent with SF1 cell projection pattern, activation of the VMHdm/c SF1 cells induced strong immediate-early gene (Fos) expression in both ventral AHN and PAG (Figure S3). Thus, we decided to investigate the behavioral responses mediated by the VMH→AHN and VMH→PAG connections.

To manipulate the VMH→AHN and VMH→PAG pathways, we virally expressed ChR2-EYFP in VMHdm/c SF1 neurons and positioned the optic fiber 0.4–0.8 mm above either the AHN or dlPAG (Figures 5A, 5G, and 5H). Given the close proximity of the VMH and AHN (approximately 1 mm apart), we used a beveled cannula to reduce the spread of light from the AHN to the VMH (Tye et al., 2011). Our in vitro measurement showed that light intensity decreased to less than 10% of that of the source at 1 mm away from the protected side of cannula ending point. Given that the minimal light intensity required to induce the behavioral change with VMH→AHN stimulation (0.4 to 3.0 mW) is comparable to that required for the VMHdm/c direct activation (0.8 to 3.5 mW), the spillover light from AHN was unlikely to activate VMHdm/c cell bodies strongly enough to induce behavioral changes directly. Whereas activating the VMH→AHN pathway (n = 25) induced immobility, running, and escape jumping similar to VMH cell body activation, VMH→PAG activation (n = 27) only increased immobility even when the stimulation intensity was high (20 ms, 20 Hz, 3.2–6.7 mW) (Figures 5I–5K; one example is shown in Figures S4C and S4D). Immobility induced by VMH→PAG appears to be more solid than VMH stimulation, as the animal ceased all movements, including those of the head and tail (Movie S5). When comparing the movement velocity during VMH, VMH→AHN, and VMH→PAG stimulation at high intensity (>3 mW) and high frequency (20 Hz), only VMH→PAG stimulation significantly reduced the locomotion velocity upon light delivery (Figures S1A–S1C). Similar to VMH cell body activation, stimulating both VMH→PAG and VMH→AHN simultaneously caused a poststimulation increase in movement velocity (Figures S1A–S1C).

In the two-chamber preference test, across all animals, the VMH→AHN pathway stimulation significantly reduced the percentage of time the animal spent in the stimulation chamber (Figure 5L; an example session is shown in Figures S4E–S4G) and decreased the percentage of time that the animal was immobile (Figure 5M). In contrast, the effect of VMH→PAG stimulation was less consistent across animals, with 5/9 animals learning to avoid the stimulation chamber (Figure 5L, left, light blue; one example in Figures S4H–S4J) while the remaining animals did not (Figure 5L, left, light red; one example in Figures S4K–S4M). The behavioral heterogeneity is also obvious when examining the level of immobility during stimulation. Avoided animals decreased immobility during stimulation, while unavoided animals showed the opposite trend (Figure 5M, left).

VMHdm/c Neurons Bifurcate to Both AHN and PAG

Given that terminal optogenetic activation could cause spiking activity in cell bodies, if VMHdm/c cells bifurcate to both AHN and PAG, the VMH→AHN-like response elicited by VMH→PAG stimulation could be caused by the backpropagation of action potentials from PAG to VMH cell bodies, which in turn recruit AHN (Jennings et al., 2013). This possibility is supported by previous retrograde tracing studies showing that nearly 50% cells in ventrolateral subdivision of VMH send collateral projections to the MPN, MEA, and/or PAG (Akesson et al., 1994). However, recent studies focusing on another hypothalamic region, the arcuate nucleus, revealed that nonoverlapping AGRP cells project to each of its downstream regions to form functionally redundant parallel pathways (Betley et al., 2013). Thus, in one scenario, the VMH→PAG and VMH→AHN may represent two independent pathways to mediate largely redundant defensive responses. Alternatively, overlapping cells in the VMHdm/c may send collateral projections to the AHN and PAG to mediate aspects of defensive responses.

To investigate the origin of the VMH→PAG- and VMH→AHN-projecting neurons, we injected cholera toxin b subunit conjugated with Alex dye 488 (CTB-488) into the PAG, and CTB-555 into the AHN in the same animal (Figures 6A–6C). Five of the 14 injected animals had both injection sites centered in the regions of interest, and were analyzed in detail (Figures S5A and S5B). On average, 46% of VMHdm/c neurons are retrogradely labeled from the PAG, while 51% of cells are labeled from the AHN (Figure 6F). Among all of the retrogradely labeled cells, 47% of PAG-projecting cells and 44% of AHN-projecting cells are dual-labeled, and 75% of them are SF1 positive (Figures 6D–6H; Table S1). Thus, activating SF1-expressing cells will recruit a large percentage of AHN, PAG, and dual-projecting VMHdm/c cells. To estimate the upper limit of our efficiency in retrogradely labeling cells, we coinjected CTB-488 and CTB-555 into the PAG (Figures S5C–S5E). Among the three well-targeted animals, we found that approximately 75% of the cells were dual-labeled (Figures S5G and S5H; Table S1). Taken together, we estimate that at least two-thirds of the VMHdm/c cells project to the PAG or AHN. Among them, over half send collateral projections to both areas.

Distinct Roles of the VMH→PAG and VMH→AHN Pathways in Mediating Defensive Response

Given that many VMHdm/c cells send projections to both PAG and AHN, it is likely that activation of the VMH→PAG pathway also activates some AHN neurons indirectly. Consistent with this hypothesis, activation of the PAG fiber terminals induced a weak increase of Fos expression in the AHN and vice versa (Figure S3). To eliminate the indirect recruitment of a collateral

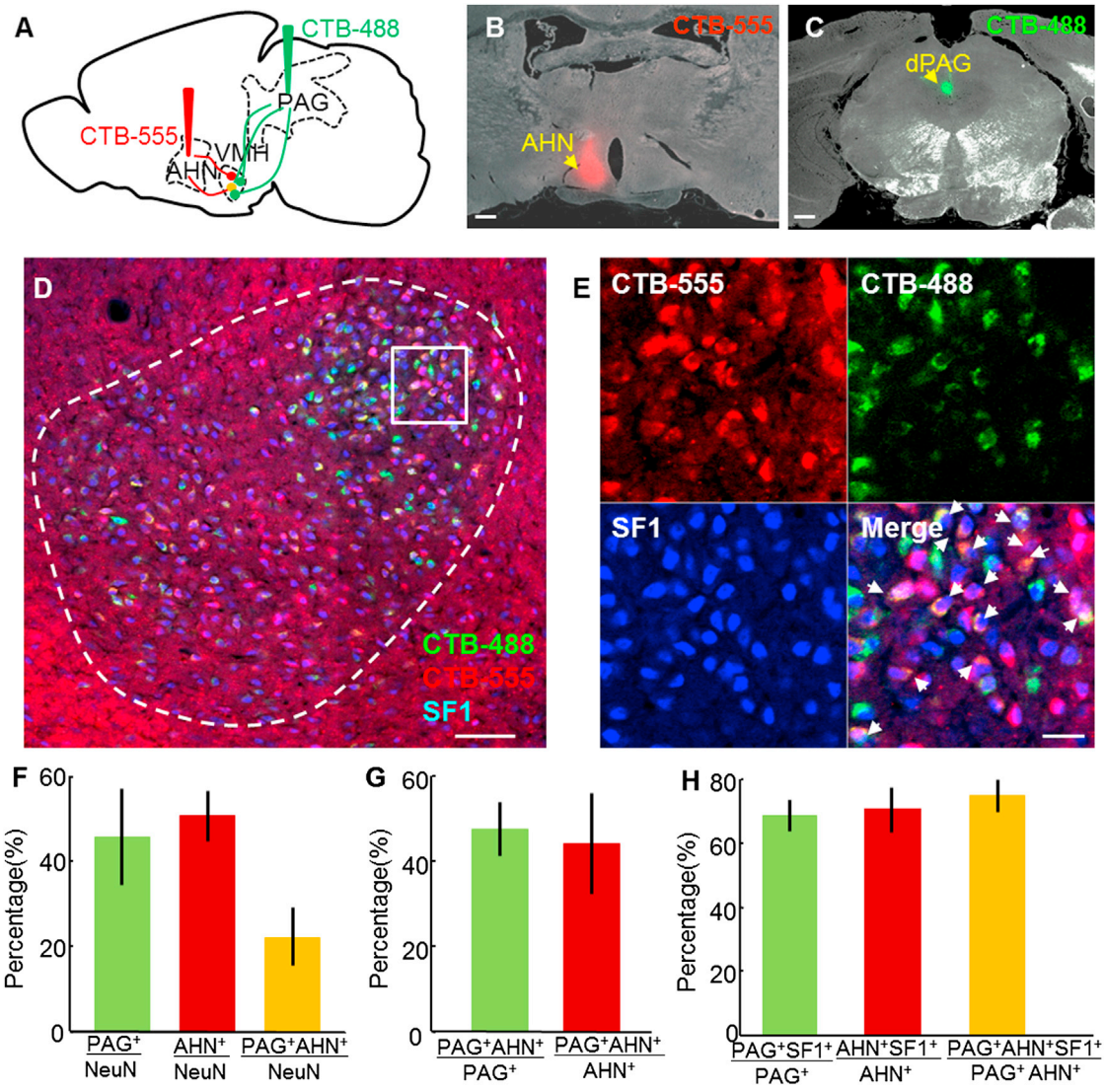

Figure 6. VMHdm/c Neurons Sent Collateral Projections to the AHN and PAG

(A) Retrograde tracing experiment.

(B and C) Injection sites in the AHN (B) and the dlPAG (C) of one animal. Scale bars, 0.5 mm.

(D) Retrogradely labeled neurons in the VMH from the PAG (green) and the AHN (red), costained with SF1 antibody (blue). Scale bar, 100 μm.

(E) Individual channels and merged view of the boxed area in (D). White arrows indicate triply labeled neurons. Scale bar, 20 μm.

(F) Percentages of PAG (green), AHN (red), and dual-projecting neurons (yellow) among all the VMHdm/c neurons.

(G) Percentages of dual-projecting neurons in PAG-projecting (green) or AHN-projecting (red) populations.

(H) Percentages of SF1-positive neurons in the PAG-, AHN-, or dual-projecting populations (n = 5 for F and G; n = 3 for H). Error bars, SE. See also Figure S5 and Table S1.

projection, we tried to block backpropagation of action potentials using several approaches, including halorhodopsin, lidocaine, tetrodotoxin, and bupivacaine (Gradinaru et al., 2010; Pereira and Morrell, 2009). Among the four tested methods, injection of 0.3 μl 4% bupivacaine completely blocked behavioral changes induced by light stimulation, and lasted for at least 45 min (Figure S6A). Importantly, bupivacaine caused little change in animals' locomotion during the RTPP test (Figure S6B, n = 11) and did not change the level of nose poking at the baseline level (Figure S6C, n = 8). Thus, bupivacaine was chosen as the method to suppress VMH activity and prevent backpropagation of action potentials.

We attempted to block VMHdm/c cell body activation with bupivacaine in 11 animals that showed clear aversion to the stimulation chamber in the RTPP test (Figure 7B). Among them, blocking was successful in six animals, as they no longer showed aversion to the stimulation chamber with VMH stimulation (Figure 7C, red). The blocking was ineffective in the remaining five

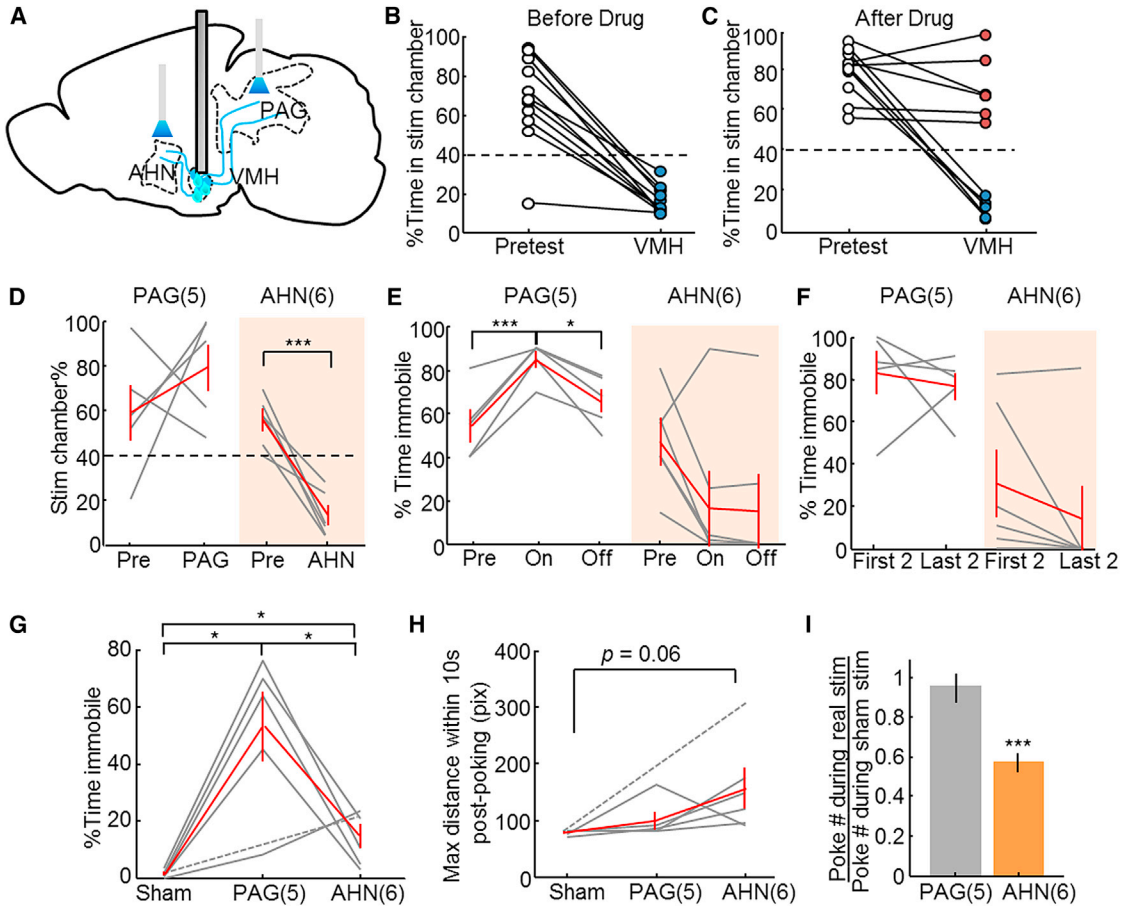

Figure 7. VMH→PAG and VMH→AHN Activation with VMH Blocking Induced Distinctive Aspects of Defensive Behaviors

(A) Schematic representation of the experiment.

(B) Before blocking, VMH stimulation induced avoidance to the stimulation chamber in all animals (n = 11).

(C) Bupivacaine injection blocked VMH stimulation-induced avoidance in 6 of 11 animals (red dots), but had no effect on the remaining five animals (blue dots).

(D) VMH→AHN stimulation (right) but not VMH→PAG stimulation (left) induced avoidance to the stimulation chamber in the RTPP test.

(E) VMH→PAG (left), but not VMH→AHN (right) stimulation increased immobility.

(F) The immobility induced by VMH→ PAG stimulation (left) is similar and high in the first two and last two entries to the stimulation chamber, whereas 5/6 animals showed low immobility during later VMH→AHN stimulation trials.

(G) In the operant punishment test, VMH→PAG stimulation induced a higher level of immobility than VMH→AHN or sham stimulation did.

(H) The animal showed a trend (p = 0.06) to move away from the poker after VMH→AHN stimulation, but not after VMH→PAG stimulation.

(I) VMH→AHN activation reduced poke number, while VMH→PAG activation did not. Gray and red lines indicate data of individual animals and population average, respectively. Error bars, SE. PAG, n = 5; AHN, n = 6; sham, n = 6. Paired t test in (D–F) and unpaired t test in (G–I): *p < 0.05, ***p < 0.001. See also Figures S6 and S7.

animals (Figure 7C, blue), which could be due to the position of the cannula ending being too medial and, thus, that the drug likely diffused into the ventricle (Figure S7A, blue dots). After confirming the successful blocking of the VMHdm/c cell bodies with bupivacaine in those six animals, we tested behavioral changes during stimulation of the VMH→PAG and VMH→AHN pathways with simultaneous VMH blocking (Figure 7A). After VMH blocking, VMH→PAG stimulation induced homogenous behavioral changes in the RTPP test: all animals significantly increased immobility during stimulation (Figure 7E, left) and showed no avoidance to the stimulation chamber, even after some had learned to avoid the chamber in the absence of VMH blocking (Figure 7D, left; one example in Figures S6D–S6I). Four additional animals were tested with VMH blocking and VMH→PAG stimulation, but with no confirmed success of VMH blocking. Histological analysis suggested that the drug was likely targeted to the VMHdm/c (Figure S6A, red open circles for unconfirmed animals) and their behavioral change was consistent with the six blocking-confirmed animals (combined data in Figures S6J and S6K). In contrast to the behavioral change observed with VMH→PAG stimulation, all animals with VMH→AHN stimulation learned to avoid the stimulation chamber even after VMH blocking (Figure 7D, right). VMH→AHN stimulation induced little immobility (Figure 7E, right), especially during later entries, 5/6 animals moved out of the chamber without any pause (Figure 7F, right). In contrast, VMH→PAG stimulation induced a high level of

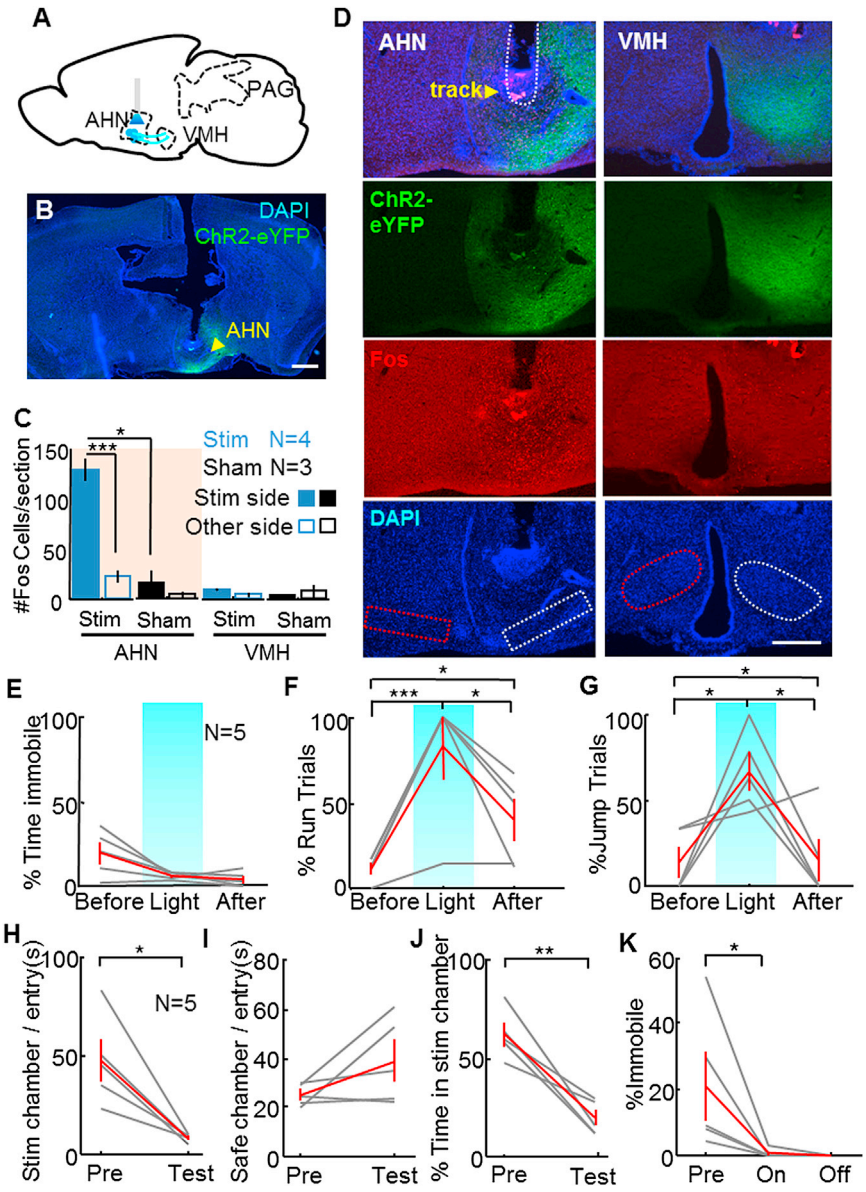

Figure 8. AHN Stimulation Induced Jump and Avoidance, but No Immobility

(A) Schematic showing injection and stimulation sites.

(B) A coronal section with cannula track and ChR2-EYFP expression (green). Scale bar, 1 mm.

(C) Average number of Fos-expressing cells per section at the AHN and VMH after AHN stimulation with light. Two-way ANOVA showed significant difference between stimulation side, stimulation condition, and their interaction term for AHN ($p < 0.01$ for all terms), but not VMH ($p > 0.1$ for all terms). Unpaired t test: $^{*}p < 0.05$, $^{***}p < 0.001$.

(D) Representative images showing the ChR2-EYFP (green) and Fos expression (red) at AHN (left) and VMH (right) after AHN light stimulation. Dashed lines mark the areas for Fos counting. Scale bar, 500 μm.

(E–G) AHN light stimulation did not change immobility level (E) but increased the percentage of trials with running (F) and jumping events (G).

(H–J) In the RTPP test, AHN stimulation decreased the time in the stimulation chamber per entry (H), did not change the percentage of time in the safe chamber per entry (I), and decreased the total percentage of time in the stimulation chamber (J).

(K) AHN stimulation decreased immobility in the RTPP test (n = 5). Paired t test for (E–K): $^{*}p < 0.05$, $^{**}p < 0.01$, $^{***}p < 0.001$.

immobility throughout the testing period (Figure 7F, left). Thus, after VMH blocking, VMH→PAG stimulation caused immobility, but not avoidance, while VMH→AHN induced little immobility, but promoted avoidance.

We further tested the potential functional segregation of the VMH→PAG and VMH→AHN pathways with punishment operant conditioning. After stable baseline poking was established, we blocked the VMH and examined poking performance when we paired poking with either VMH→PAG or VMH→AHN stimulation. We found that VMH→PAG stimulation caused a significantly higher level of immobility than VMH→AHN or sham stimulation (Figure 7G). During VMH→PAG stimulation, test animals paused in the middle of licking and resumed normal activity afterward. During VMH→AHN stimulation, animals continued to lick. However, after several paired stimulations, they moved away from the poker and stayed away for tens to hundreds of seconds (Figure 7H). As a result, VMH→AHN stimulation reduced the total number of pokes significantly (Figure 7I, orange bar). In contrast, despite the short pause of movement elicited by VMH→PAG stimulation, animals showed no avoidance to the poker after VMH→PAG stimulation (Figure 7H), and the overall poke number did not decrease relative to that under the sham condition (Figure 7I, gray bar). This result is consistent with the functional results from the RTPP test, suggesting distinct roles of the VMH→PAG and VMH→AHN pathways in mediating the stereotyped immobility and flexible avoidance behavior in the face of danger.

Optogenetic Activation of AHN Induced Running, Escape Jumping, and Avoidance, but Not Immobility

Although the AHN represents the most prominent anterior target of the VMHdm/c SF1 cells, axons from the VMHdm/c also course through the AHN and reach more anterior and dorsal structures, such as the MPN and the BNST. To investigate whether the behavioral change induced by VMH→AHN activation is solely mediated by fibers of passage, we virally expressed ChR2 in the ventral AHN area and examined the behavioral changes induced by light (Figure 8A). Histological analysis showed that the ChR2 was expressed mainly in the ventral AHN in five of the eight injected animals that were included in the analysis

(Figure 8B). Interestingly, although we observed ChR2-EYFP axons in the VMHdm/c, which is consistent with the known afferent pattern of the AHN (Saper et al., 1978), little Fos expression was observed in the VMHdm/c after AHN activation by light, whereas strong Fos expression was observed in the AHN itself (Figures 8C and 8D). This differential Fos induction pattern also ensured that the virus did not spread to the VMH to cause its direct activation.

In contrast to the motor responses induced by VMHdm/c activation, activating the ventral AHN failed to induce immobility. Instead, upon stimulation, animals increased locomotion, reared toward the cage wall, and jumped repeatedly (Figure 8E; Movie S6). In addition, in the RTPP test, all animals showed strong avoidance to the stimulation chamber. Once the stimulation session started, all animals learned to move out of the stimulation chamber within the first three entries (Figure 8H; Movie S7). Across animals, the percentage of time in the stimulation chamber decreased from 62% in the pretest to 19% during test (Figure 8J). Consistent with the home cage results, animals showed no immobility during stimulation (Figure 8K). These results reveal differential roles of VMHdm and AHN in mediating defensive behaviors, and support the notion that escape jumping and avoidance induced by VMHdm/c stimulation is, at least in part, mediated by projection of the VMHdm/c to the AHN.

DISCUSSION

We used optogenetic methods to show that VMHdm/c activation induces complex somatomotor and autonomic responses that resemble animals' natural behaviors in the face of danger. The responses include pupil dilation, an increase in breathing rhythm, changes in HR and HRV, immobility, running, escape jumping, hiding, and avoidance. Combining pathway-specific activation and cell body inactivation, we found that VMH→PAG activation elicits immediate stereotyped immobility, but not avoidance, while VMH→AHN activation promotes avoidance. Consistent with the pathway activation results, direct activation of ventral AHN cells elicits avoidance, but not immobility. Interestingly, many VMHdm/c cells send collateral projections to both the AHN and PAG, suggesting a one-to-many wiring configuration to coordinate multiple aspects of defensive behavior.

The Defense-like Motor and Autonomic Responses Induced from VMHdm/c

In our study, we observed immobility in all 31 experimental animals during VMHdm/c light stimulation, despite the fact that the ChR2 expression level and optic fiber position varied among animals. This consistent behavioral change is likely contributed by both the relatively precise and restricted ChR2 expression in the VMHdm/c using SF1:CRE mouse line and the dominance of the defensive behaviors among all innate behaviors. Given that SF1 is also expressed in VMHvl to a small extent, some of the animals showed ChR2 expression in both the VMHdm and VMHvl. However, the VMHvl is unlikely to be responsible for the induced defensive behavior, as our previous studies showed that VMHvl activation elicits aggressive behaviors (Lin et al., 2011). Only when the virus spread into the VMHdm/c were defensive-like behaviors elicited rather than attack ones (Lin et al., 2011). In this study, we never observed any light-evoked attack, indicating that defensive behavior completely overrides aggressive behavior when neural substrates for both are simultaneously activated.

The light-induced cardiovascular response changed from tachycardia to bradycardia as the stimulation intensity increased, despite the fact that immobility was induced under both conditions. This indicates that the cardiovascular response and immobility are dissociable. Consistent with this observation, both the tachycardia and bradycardia responses have been reported to accompany immobility under natural threatening conditions. For example, exposure to an electric-shock-paired tone induced immobility and a dramatic increase in HR (Stiedl and Spiess, 1997), while HR was strongly suppressed when the animal experienced tonic immobility (playing dead) during predator exposure (Hofer, 1970). Thus, VMHdm/c neurons may mediate immobility under various contexts that require either an increase or a decrease in HR. Future studies aimed at understanding the response of the VMHdm/c cell toward natural threat will help test these hypotheses.

The Hypothalamic Defense Circuit

Based on tracing and immediate-early gene studies, the medial hypothalamic defense circuit is proposed to contain three nuclei: the AHN, VMHdm/c, and PMd (Martinez et al., 2008). However, it remains unclear how the danger-associated sensory information is processed by these areas to elicit defensive behaviors. Our studies provide some new insight into the organization of the medial hypothalamic defense circuit.

At the input level, among the three defense nuclei, VMHdm/c receives the most abundant sensory inputs from regions outside of the hypothalamus, including olfactory inputs via the MEA, auditory and visual inputs via the posterior part of the basomedial amygdala, and somatosensory inputs (especially pain) via the parabrachial nucleus (Canteras et al., 1995; Petrovich et al., 1996; Saper and Loewy, 1980). At the output, although previous studies suggested that the VMH pathway to midbrain involves a synapse in the AHN (Fuchs et al., 1985), our study demonstrated that the VMH to PAG projection is direct and can induce immediate immobility (Figure S8A). This is somewhat surprising as the VMHdm/c mainly projects to dlPAG, which is traditionally believed to be an active emotional coping zone that mediates running and jumping (Bandler and Keay, 1996). Nevertheless, based on the connectivity and our functional manipulation results, VMHdm/c appears to be well positioned to detect predator-related sensory cues and to quickly suppress locomotion to minimize the risk of self exposure.

Classical electrical stimulation studies showed that the AHN and VMH elicit similar behavioral responses, such as flight and escape jumping (Lammers et al., 1988). Tracing studies revealed strong reciprocal connections between these two areas (Canteras et al., 1994; Saper et al., 1978). Thus, it appears that the VMHdm/c and AHN may have redundant roles in mediating defense. However, our studies revealed clear functional distinction between these two areas: while activation of VMHdm/c induced immediate immobility and avoidance, AHN activation induced only avoidance. Furthermore, while VMH stimulation is highly effective in inducing Fos expression in the AHN (Figure S3),

AHN stimulation induced little Fos at the VMH (Figures 8C and 8D). Consistent with our Fos results, an online gene expression database (http://www.brain-map.org) indicates that VMHdm/c cells are largely glutamatergic, while the AHN contains mostly GABAergic neurons (Figure S8B). Thus, although AHN and VMH are bidirectionally connected, the information transfer between these two areas is likely to be directional.

Surprisingly, although the VMH→AHN and VMH→PAG pathways mediate distinct aspects of the defensive responses, at least 50% of AHN-projecting cells are estimated to send a collateral projection to PAG and vice versa, offering an alternative circuit organization scheme from those proposed recently. In one study, nonoverlapping AGRP neurons were shown to target distinct downstream targets, several of which evoke similar feeding responses, forming a one-to-one and redundant output configuration (Betley et al., 2013). In another study, each of the three adBNST downstream areas were shown to receive inputs from separate adBNST subpopulations, and mediate an independent feature of anxiolysis, forming a one-to-one and nonredundant configuration (Kim et al., 2013). In contrast, here we showed that VMHdm/c neurons employ a one-to-many but nonredundant organization scheme: VMHdm/c neurons send collateral projections to AHN and dlPAG, but each pathway mediates distinct aspect of defensive behaviors. Given that collateral projections exist in many hypothalamic regions and elsewhere, this one-to-many circuit configuration is well suited to coordinate multiple aspects of a behavior.

EXPERIMENTAL PROCEDURES

Animals

Subjects were SF1:CRE transgenic male and female mice (provided by Dr. Lowell's group at Harvard; 8–24 weeks) and C57BL/6N male and female mice (10–16 weeks, Charles River Laboratories). Care and experimental manipulations of animals were approved by the Institutional Animal Care and Use Committee of NYU Langone Medical Center in compliance with the NIH guidelines.

Stereotactic Surgery and Injection

SF1:Cre mice were injected unilaterally with AAV2/2 ER1α:DIO-ChR2-EYFP into VMH (–4.5 mm anterior-posterior [AP], +0.4 mm medial-lateral [ML], 5.4 mm dorsal-ventral [DV]) (Chan et al., 2007). Wild-type mice were injected with a mixture of AAV2/2 CMV:CRE and AAV2/2 ER1α:DIO-ChR2-EYFP into AHN (–3.5 mm AP, 0.4 mm ML,–5.4 mm DV). A double cannula (1 mm center-to-center distance, Plastics One) was implanted 0.4–0.8 mm above AHN and VMH, and an optic fiber with 1.25 mm ferrule was implanted 0.5 mm above dlPAG (–7.7 mm AP, 0.2 mm ML, –1.9 mm DV). For in vivo recording, an optrode attached to a microdriver was implanted in the VMHdm/c. For tracing, 0.12 μl CTB-555 (Life Technologies) was injected into the AHN and 0.12 μl CTB-488 was injected into dlPAG. For inactivation of the VMHdm/c, 4% bupivacaine (Sigma) dissolved in 0.9% saline was injected through the implanted cannula. Behavioral tests were performed 15 min after injection.

Optrode Recording and Analysis

Two weeks after injection, the implanted optrode was connected to a 16-channel headstage and a 105 μm multimode optic fiber. In freely moving animals, neural activity was recorded continuously using a commercial system (Tucker-Davis Technologies) as light stimulation (Shanghai dream laser, 473 nm, 1 ms, 5 Hz) was delivered through the optic fiber. The direct activation of ChR2-expressing cell was determined by its latency, jitter, as well as its waveform. The placement of the optrode was examined histologically.

Behavioral Tests and Analysis

During the home cage test, blue light with low or high intensity and a range of frequency (5, 10, 15, and 20 Hz) was delivered to the VMH, AHN, or PAG. The low intensity refers to the minimal intensity required to induce behavioral changes, ranging from 0.8 to 3.5 mW. The high intensity refers to three times the minimal intensity, and up to 6 mW. Each stimulation trial lasted for 60 s unless we observed jumping, which would terminate the trial. In the hiding box test, after 10 min habituation, animals were stimulated with low intensity (20 ms, 20 Hz, 1–1.3 mW, 60 s) or sham light pulses whenever they reached one designated corner away from the hiding box. Animals also were tested with the same stimulation condition in the absence of hiding box. For the RTPP test, after 10 min of habituation, the animal was stimulated (3 s on, 2 s off) at the brain site of interest (VMH, AHN, PAG) whenever it entered a designated chamber until it moved out. In the punishment operant conditioning test, animals were deprived of water for 19 hr, and then trained to associate nose poking with water delivery for 30 min each day. Once the animal reached a steady poking rate (poking number within ± 10% for 2 consecutive days), 2 s light pulses were delivered 0.8 s after each poke during the test session. Paired t test was used to compare behavioral parameters with and without light. When multiple pairs of conditions were compared (e.g., before, during, and after light), the p value was adjusted based on false discovery rate (FDR) 0.05. When shown, an error bar means SE.

Tracking and Annotation Comparison

Custom tracking software written in MATLAB (MathWorks) was used to determine the instantaneous position of the recorded mouse based on side-view and top-view videos (Dollar et al., 2010). The instantaneous xy and z velocities of each frame were calculated to determine immobility, running, and jumping events based on a set criterion. The correlation coefficient between human/human annotations and human/computer annotations were compared to evaluate the performance of our autoannotation program.

Autonomic Responses

Pupillary and respiratory responses were measured when animals were head fixed. Low-intensity light (0.8–1.7 mW, 20 ms, 20 Hz, 20 s), high-intensity light (2.4–5.1 mW), and sham light (0 mW) were interleaved and delivered to VMH (ten times each). Pupillary responses were recorded under infrared lighting. The pupil size of each frame was determined using a custom-written MATLAB program. Breathing rate was counted manually, based on the chest movement captured on the video. Cardiovascular responses were measured in free-moving animals using three insulated multistranded stainless steel wire leads (A-M system, 793200) subcutaneously placed in the animal's left arm, right arm, and right leg. The raw electrocardiogram (ECG) signals were band-pass filtered, and the peak of the ECG trace that corresponds to individual heartbeat was determined by a custom-written MATLAB program. The HR was calculated as the inverse of interbeat interval. The HRV was calculated as the SD of HR divides the mean of HR.

Histology

Standard immunohistochemistry procedures were followed to obtain and stain the 30 μm brain sections for all mice. The 2.5× or 5× fluorescent images were acquired to determine cannula, optic fiber, and optrode placements and tracer injection sites. For Fos cell counting, 10× fluorescent images were used; 20× confocal images were obtained to quantify colocalization of CTB tracers. Cells were manually counted after selecting regions of interest based on DAPI or NeuN staining. To quantify YFP distribution in the VMHdm/c versus VMHvl, the ratio of the accumulated pixel values in green channel in VMHdm/c and VMHvl was calculated for each section, and then averaged across sections for each animal.

See Supplemental Experimental Procedures for more details.

SUPPLEMENTAL INFORMATION

Supplemental Information includes eight figures, one table, Supplemental Experimental Procedures, and seven movies and can be found with this article online at http://dx.doi.org/10.1016/j.neuron.2014.12.025.

AUTHOR CONTRIBUTIONS

D.L. designed the research. L.W. performed the research. I.Z.C and D.L. performed unpublished pilot experiments. D.L. and L.W. analyzed data and wrote the paper.

ACKNOWLEDGMENTS

We thank B. Lowell for providing the SF1-CRE mice and G. Fishell for providing the RCE:loxP mice. We also thank K. Deisseroth for ChR2-EYFP viral constructs; J.E. Feng and B.C. Chang for helping construct the optrodes; K. Ferguson for assistance with the behavioral tests; and P. Dollar for advice on optimizing the tracking program. Finally, we thank N.S. Canteras, J.E. LeDoux, A.L. Falkner, K. Hashikawa, and L.C. Wong for helpful conversations, and P. Hare and S. Tranguch for editorial comments. This work was supported by Esther A. & Joseph Klingenstein Fund (D.L.), Whitehall Foundation (D.L.), Sloan Foundation (D.L.), McKnight Foundation (D.L.), and an NIH grant (1R01MH101377 to D.L.).

Received: June 17, 2014
Revised: November 7, 2014
Accepted: December 9, 2014
Published: March 5, 2015

REFERENCES

Akesson, T.R., Ulibarri, C., and Truitt, S. (1994). Divergent axon collaterals originate in the estrogen receptive ventromedial nucleus of hypothalamus in the rat. J. Neurobiol. *25*, 406–414.

Bandler, R., and Keay, K.A. (1996). Columnar organization in the midbrain periaqueductal gray and the integration of emotional expression. Prog. Brain Res. *107*, 285–300.

Bard, P. (1928). A diencephalic mechanism for the expression of rage with special reference to the sympathetic nervous system. Am. J. Physiol. *84*, 490–515.

Betley, J.N., Cao, Z.F., Ritola, K.D., and Sternson, S.M. (2013). Parallel, redundant circuit organization for homeostatic control of feeding behavior. Cell *155*, 1337–1350.

Blanchard, R.J., Parmigiani, S., Bjornson, C., Masuda, C., Weiss, S.M., and Blanchard, D.C. (1995). Antipredator behavior of Swiss-Webster mice in a visible burrow system. Aggress. Behav. *21*, 123–136.

Blanchard, R.J., Hebert, M.A., Ferrari, P.F., Palanza, P., Figueira, R., Blanchard, D.C., and Parmigiani, S. (1998). Defensive behaviors in wild and laboratory (Swiss) mice: the mouse defense test battery. Physiol. Behav. *65*, 201–209.

Boyden, E.S., Zhang, F., Bamberg, E., Nagel, G., and Deisseroth, K. (2005). Millisecond-timescale, genetically targeted optical control of neural activity. Nat. Neurosci. *8*, 1263–1268.

Brandão, M.L., Zanoveli, J.M., Ruiz-Martinez, R.C., Oliveira, L.C., and Landeira-Fernandez, J. (2008). Different patterns of freezing behavior organized in the periaqueductal gray of rats: association with different types of anxiety. Behav. Brain Res. *188*, 1–13.

Burgos-Artizzu, X.P., Dollár, P., Lin, D., Anderson, D.J., and Perona, P. (2012). Social behavior recognition in continuous video. Proceedings of the 2012 IEEE Conference on Computer Vision and Pattern Recognition, 1322–1329.

Canteras, N.S., and Swanson, L.W. (1992). The dorsal premammillary nucleus: an unusual component of the mammillary body. Proc. Natl. Acad. Sci. USA *89*, 10089–10093.

Canteras, N.S., Simerly, R.B., and Swanson, L.W. (1994). Organization of projections from the ventromedial nucleus of the hypothalamus: a Phaseolus vulgaris-leucoagglutinin study in the rat. J. Comp. Neurol. *348*, 41–79.

Canteras, N.S., Simerly, R.B., and Swanson, L.W. (1995). Organization of projections from the medial nucleus of the amygdala: a PHAL study in the rat. J. Comp. Neurol. *360*, 213–245.

Chan, E., Kovacevíc, N., Ho, S.K.Y., Henkelman, R.M., and Henderson, J.T. (2007). Development of a high resolution three-dimensional surgical atlas of the murine head for strains 129S1/SvImJ and C57Bl/6J using magnetic resonance imaging and micro-computed tomography. Neuroscience *144*, 604–615.

Dhillon, H., Zigman, J.M., Ye, C., Lee, C.E., McGovern, R.A., Tang, V., Kenny, C.D., Christiansen, L.M., White, R.D., Edelstein, E.A., et al. (2006). Leptin directly activates SF1 neurons in the VMH, and this action by leptin is required for normal body-weight homeostasis. Neuron *49*, 191–203.

Dielenberg, R.A., Hunt, G.E., and McGregor, I.S. (2001). "When a rat smells a cat": the distribution of Fos immunoreactivity in rat brain following exposure to a predatory odor. Neuroscience *104*, 1085–1097.

Dollar, P., Welinder, P., and Perona, P. (2010). Cascaded pose regression. Proceedings of the 2010 IEEE Conference on Computer Vision and Pattern Recognition, 1078–1085.

Eilam, D. (2005). Die hard: a blend of freezing and fleeing as a dynamic defense—implications for the control of defensive behavior. Neurosci. Biobehav. Rev. *29*, 1181–1191.

Fernandez De Molina, A., and Hunsperger, R.W. (1962). Organization of the subcortical system governing defence and flight reactions in the cat. J. Physiol. *160*, 200–213.

Franklin, K.B.J., and Paxinos, G. (2008). The Mouse Brain in Stereotaxic Coordinates. (Academic Press).

Fuchs, S.A., Edinger, H.M., and Siegel, A. (1985). The role of the anterior hypothalamus in affective defense behavior elicited from the ventromedial hypothalamus of the cat. Brain Res. *330*, 93–107.

Gradinaru, V., Zhang, F., Ramakrishnan, C., Mattis, J., Prakash, R., Diester, I., Goshen, I., Thompson, K.R., and Deisseroth, K. (2010). Molecular and cellular approaches for diversifying and extending optogenetics. Cell *141*, 154–165.

Hofer, M.A. (1970). Cardiac and respiratory function during sudden prolonged immobility in wild rodents. Psychosom. Med. *32*, 633–647.

Höfle, M., Pomper, U., Hauck, M., Engel, A.K., and Senkowski, D. (2013). Spectral signatures of viewing a needle approaching one's body when anticipating pain. Eur. J. Neurosci.

Jennings, J.H., Sparta, D.R., Stamatakis, A.M., Ung, R.L., Pleil, K.E., Kash, T.L., and Stuber, G.D. (2013). Distinct extended amygdala circuits for divergent motivational states. Nature *496*, 224–228.

Kim, S.Y., Adhikari, A., Lee, S.Y., Marshel, J.H., Kim, C.K., Mallory, C.S., Lo, M., Pak, S., Mattis, J., Lim, B.K., et al. (2013). Diverging neural pathways assemble a behavioural state from separable features in anxiety. Nature *496*, 219–223.

Lammers, J.H., Kruk, M.R., Meelis, W., and van der Poel, A.M. (1988). Hypothalamic substrates for brain stimulation-induced patterns of locomotion and escape jumps in the rat. Brain Res. *449*, 294–310.

Lin, D., Boyle, M.P., Dollar, P., Lee, H., Lein, E.S., Perona, P., and Anderson, D.J. (2011). Functional identification of an aggression locus in the mouse hypothalamus. Nature *470*, 221–226.

Lindberg, D., Chen, P., and Li, C. (2013). Conditional viral tracing reveals that steroidogenic factor 1-positive neurons of the dorsomedial subdivision of the ventromedial hypothalamus project to autonomic centers of the hypothalamus and hindbrain. J. Comp. Neurol. *521*, 3167–3190.

Lipp, H.P., and Hunsperger, R.W. (1978). Threat, attack and flight elicited by electrical stimulation of the ventromedial hypothalamus of the marmoset monkey *Callithrix jacchus*. Brain Behav. Evol. *15*, 260–293.

Martinez, R.C., Carvalho-Netto, E.F., Amaral, V.C., Nunes-de-Souza, R.L., and Canteras, N.S. (2008). Investigation of the hypothalamic defensive system in the mouse. Behav. Brain Res. *192*, 185–190.

McClellan, K.M., Parker, K.L., and Tobet, S. (2006). Development of the ventromedial nucleus of the hypothalamus. Front. Neuroendocrinol. *27*, 193–209.

Pereira, M., and Morrell, J.I. (2009). The changing role of the medial preoptic area in the regulation of maternal behavior across the postpartum period: facilitation followed by inhibition. Behav. Brain Res. *205*, 238–248.

Petrovich, G.D., Risold, P.Y., and Swanson, L.W. (1996). Organization of projections from the basomedial nucleus of the amygdala: a PHAL study in the rat. J. Comp. Neurol. *374*, 387–420.

Risold, P.Y., Canteras, N.S., and Swanson, L.W. (1994). Organization of projections from the anterior hypothalamic nucleus: a Phaseolus vulgaris-leucoagglutinin study in the rat. J. Comp. Neurol. *348*, 1–40.

Saper, C.B., and Loewy, A.D. (1980). Efferent connections of the parabrachial nucleus in the rat. Brain Res. *197*, 291–317.

Saper, C.B., Swanson, L.W., and Cowan, W.M. (1978). The efferent connections of the anterior hypothalamic area of the rat, cat and monkey. J. Comp. Neurol. *182*, 575–599.

Schmitt, P., Di Scala, G., Brandao, M.L., and Karli, P. (1985). Behavioral effects of microinjections of SR 95103, a new GABA-A antagonist, into the medial hypothalamus or the mesencephalic central gray. Eur. J. Pharmacol. *117*, 149–158.

Silva, B.A., Mattucci, C., Krzywkowski, P., Murana, E., Illarionova, A., Grinevich, V., Canteras, N.S., Ragozzino, D., and Gross, C.T. (2013). Independent hypothalamic circuits for social and predator fear. Nat. Neurosci. *16*, 1731–1733.

Silveira, M.C., and Graeff, F.G. (1988). Defense reaction elicited by microinjection of kainic acid in the medial hypothalamus of the rat. Braz. J. Med. Biol. Res. *21*, 569–571.

Stiedl, O., and Spiess, J. (1997). Effect of tone-dependent fear conditioning on heart rate and behavior of C57BL/6N mice. Behav. Neurosci. *111*, 703–711.

Tye, K.M., Prakash, R., Kim, S.Y., Fenno, L.E., Grosenick, L., Zarabi, H., Thompson, K.R., Gradinaru, V., Ramakrishnan, C., and Deisseroth, K. (2011). Amygdala circuitry mediating reversible and bidirectional control of anxiety. Nature *471*, 358–362.

Wilent, W.B., Oh, M.Y., Buetefisch, C.M., Bailes, J.E., Cantella, D., Angle, C., and Whiting, D.M. (2010). Induction of panic attack by stimulation of the ventromedial hypothalamus. J. Neurosurg. *112*, 1295–1298.